Electron Heating in Magnetosheath Turbulence: Dominant Role of the Parallel Electric Field within Coherent Structures

Qianyun Xu[1,2], Meng Zhou[1,2], Wenqing Ma[2], Jiansen He[3],
Shiyong Huang[4], Zhihong Zhong[1,2], Ye Pang[2], Xiaohua Deng[2]

1. Department of Physics, School of Physics and Materials Science, Nanchang University, Nanchang 330031, People's Republic of China;
2. Institute of Space Science and Technology, Nanchang University, Nanchang 330031, People's Republic of China;
3. School of Earth and Space Sciences, Peking University, Beijing 100871, People's Republic of China;
4. School of Electronic Information, Wuhan University, Wuhan, People's Republic of China;

Key points:

1. Electrons are primarily accelerated by the parallel electric field in the magnetosheath turbulence.
2. The $E_{||}$ acceleration mostly occurs within the coherent structures through Joule-type dissipation.
3. The average $E_{||}$ acceleration rate increases with the decreasing local spatial scale.

Abstract

How are particles being energized by turbulent electromagnetic fields is an outstanding question in plasma physics and astrophysics. This paper investigates the electron acceleration mechanism in strong turbulence ($\delta B/B_0 \sim 1$) in the Earth's magnetosheath based on the novel observations of the Magnetospheric Multiscale (MMS) mission. We find that electrons are magnetized in turbulent fields for the majority of the time. By directly calculating the electron acceleration rate from Fermi, betatron mechanism, and parallel electric field, it is found that electrons are primarily accelerated by the parallel electric field within coherent structures. Moreover, the acceleration rate by parallel electric fields increases as the spatial scale reduces, with

the most intense acceleration occurring over about one ion inertial length. This study is an important step towards fully understanding the turbulent energy dissipation in weakly collisional plasmas.

Plain language summary

The magnetosheath is one of the most turbulent environments in near-Earth space, which is very beneficial to the study of collisionless turbulent plasma. The mechanism of turbulent energy dissipation and the consequent plasma heating is not fully understood. The Magnetosphere Multiscale mission provides high-time cadence data and simultaneous multi-spacecraft measurements at very small inter-spacecraft separations. That can measure important quantities related to dissipation and heating at kinetic scales. This paper investigates how electrons are being accelerated through the dissipation of magnetic energy in nonlinear turbulence in the Earth's magnetosheath. We classify the acceleration mechanisms into three types: Fermi mechanism, betatron mechanism, and $E_{||}$ acceleration. By directly calculating and comparing these mechanisms, we find electrons are predominantly accelerated by parallel electric fields within coherent structures. The $E_{||}$ acceleration is the most effective around the ion inertial length.

1. Introduction

Energy cascade is one of the most prominent features of turbulence. Energy is injected at large scales, like fluid scales, then cascades to small scales through non-linear interactions, and finally dissipated at kinetic scales, leading to plasma heating and particle acceleration and the formation of suprathermal tails in the particle energy spectrum (Kiyani et al., 2015). Space plasma is typical of weak collisionality; hence collisionless mechanisms play a critical role in turbulent energy dissipation in space plasmas (Matthaeus et al., 2015; Chen 2016; Howes 2017). How the particles are heated/accelerated by turbulence is one of the most outstanding questions in plasma turbulence; however, the mechanism of turbulent energy dissipation and the consequent plasma heating is not fully understood after decades of intensive study.

Different types of acceleration mechanisms have been proposed to explain plasma

heating by the turbulent cascade in collisionless plasma. These mechanisms can be generally classified into two categories: resonant acceleration and non-resonant acceleration. The dissipation of waves is usually due to the energy transfer to energizing particles caused by field and particle resonance, which can work over a long distance and a long time. It includes Landau damping, cyclotron damping, and transit-time damping (Chandran et al., 2010; Dmitruk et al., 2004a; Sahraoui et al., 2009; Isenberg & Hollweg 1983; Gary et al., 2000; Isenberg 2001; Marsch & Tu 2001; Klein et al., 2017). Previous studies have found clues of this resonant acceleration in space plasma turbulence. He et al. (2015a, 2015b) suggested that solar wind ions are heated by Landau damping and cyclotron damping by identifying characteristic signatures of these resonances in the ion velocity distribution functions. Recently, in situ signature of cyclotron resonant heating in the solar wind turbulence is observed by Parker Solar Probe observations (Bowen et al., 2022). Chen et al. (2019) presented direct evidence for Landau damping in magnetosheath turbulence by using the novel field-particle correlation technique. The Landau damping mechanism for electron heating is further confirmed by examining more events in the magnetosheath using the same field-particle correlation method (Afshari et al., 2021).

One typical non-resonant acceleration is stochastic heating, which heats plasma when the motion of particles becomes chaotic as the amplitude of electromagnetic field fluctuations, at scales comparable to the gyro-scale, exceeds a critical value (Chandran et al., 2010; Vech et al., 2017). It is found that acceleration and dissipation also occur in coherent structures, such as current sheets (Retinò et al., 2007; Dmitruk et al., 2004b; Osman et al., 2012), magnetic islands (Huang et al., 2016), small-scale vortices (Alexandrova & Saur 2008), and magnetic holes (Huang et al., 2017a, 2017b; Zhong et al., 2019), etc. It is suggested that magnetic reconnection occurring within the current sheets in turbulence provides an important pathway for energy dissipation (Osman et al., 2014; Zhou et al., 2021). The correlation between energy dissipation and localized coherent structures indicates that energy dissipation may occur non-uniformly.

The motivation of this study is to investigate the acceleration and heating of electrons in plasma turbulence. Different from Chen et al. (2019) and Afshari et al. (2021), the

turbulent interval we examine in this paper has large fluctuations with $\delta B/B_0 \sim 1$. In addition, we not only quantify the electron acceleration rate by the parallel electric field, as has been done by Chen et al. (2019) and Afshari et al. (2021), but also quantify the acceleration by the perpendicular electric field. The electron acceleration rates are evaluated under the guiding center approximation. We have used the data from the Magnetospheric Multiscale (MMS) mission, which provides high-time cadence data and simultaneous multi-spacecraft measurements at very small inter-spacecraft separations. This combination enables the study of the nature of dissipation at kinetic scales with an unprecedented level of accuracy and resolution. The FGM magnetic field instruments (Russell et al., 2016), EDP electric field instruments (Ergun et al., 2016; Lindqvist et al., 2016), and FPI ion and electron detectors (Pollock et al., 2016) provide the high-resolution data required to characterize signatures of dissipation and heating.

2. Methodology

Here we employ the method that has been used to calculate the acceleration rate in reconnection. This method considers the particle energy gain under guiding center approximation (Dahlin et al., 2014; Zhou et al., 2018; Zhong et al., 2020; Ma et al., 2020, 2022). The integrated energy gain of electrons in a unit volume per unit time for betatron acceleration is given by:

$$W_b = P_{e\perp}\boldsymbol{v}_{\boldsymbol{E}\times\boldsymbol{B}} \cdot \frac{\boldsymbol{\nabla B}}{B} + \frac{P_{e\perp}}{B}\frac{\boldsymbol{\partial B}}{\boldsymbol{\partial} t} \quad (1)$$

where $P_{e\perp}$ is the perpendicular electron pressure, $\boldsymbol{v}_{\mathbf{E}\times\mathbf{B}}$ is the E×B drift speed, $\boldsymbol{\nabla B}$ is the gradient of the total magnetic field. We refer to W_b as the betatron acceleration rate hereafter. Betatron acceleration might be efficient in magnetosheath turbulence, which usually involves large-amplitude |B| fluctuations, such as magnetic holes and magnetic peaks (e.g., Huang et al., 2017a, 2017b; Yao et al., 2018).

The Fermi acceleration rate is calculated by

$$W_f = \left(P_{e||} + n_e m_e v_{e||}^2\right)\boldsymbol{v}_{\boldsymbol{E}\times\boldsymbol{B}} \cdot (\boldsymbol{b} \cdot \boldsymbol{\nabla b}) \quad (2)$$

where $P_{e||}$ is the electron parallel pressure, $v_{e||}$ is the electron parallel bulk velocity and **b** is the unit vector of the magnetic field. Fermi acceleration is essentially caused by the

curvature drift in motional curved field lines. In situ observations in the magnetosheath suggest that curvature drift acceleration may be important for particle energization in magnetized turbulence (Bandyopadhyay et al., 2020; Huang et al., 2020).

The $E_{||}$ acceleration rate, which is caused by the parallel electric field, is given by

$$W_{E||} = J_{e||}E_{||} + \frac{\beta_{e\perp}}{2}J_{||}E_{||} \quad (3)$$

where $\beta_{e\perp}$ is the ratio between the perpendicular electron pressure and the magnetic pressure, $J_{||}$ is the total parallel current density and $J_{e||}$ is the parallel current carried by electrons. The presence of $\frac{\beta_{e\perp}}{2}J_{||}E_{||}$ is to eliminate the work caused by the parallel magnetization drift.

Betatron and Fermi mechanisms cause the heating of plasmas while $E_{||}$ leads to not only plasma heating but also plasma bulk acceleration. The heating of plasma by $E_{||}$ can be understood by examining the electron momentum equation:

$$E_{||} = -\frac{1}{en}(\boldsymbol{\nabla}\cdot\mathbf{P}_e)_{||} - \frac{m_e}{e}\left(\frac{d\boldsymbol{v_e}}{dt}\right)_{||} \quad (4)$$

where e is the unit charge, n is the number density, $\mathbf{v}_e$ is the electron bulk velocity and $\mathbf{P}_e$ is the electron pressure tensor. The relationship between the parallel electric field and the electron energy gain can be obtained by multiplying Eq. (4) by $-nev_{e||}$:

$$-nev_eE_{||} = v_{e||}(\boldsymbol{\nabla}\cdot\mathbf{P}_e)_{||} + nm_ev_{e||}\left(\frac{d\boldsymbol{v_e}}{dt}\right)_{||} \quad (5)$$

The first term on the RHS of Eq. (5) contributes to the thermal energy increase of electrons, i.e., electron heating, while the second term on the RHS of Eq. (5) is related to the electron bulk velocity variation.

Equations (1) – (3) can be used to evaluate the acceleration rates for the three different types of mechanisms when the electrons satisfy the guiding center approximation, i.e., they are magnetized, or say, the 1st adiabatic invariant is conserved. To test this criterion, we calculate κ (Büchner & Zelenyi 1989):

$$\kappa_{curv} = \sqrt{R_c/\rho_e} \quad (6)$$

where R_c is the curvature radius of the magnetic field, and ρ_e is the electron gyration radius, which is calculated by using four times the electron temperature, higher than the energy of most electrons in the magnetosheath. When $\kappa>3$, electrons of the specific

147 energy are considered to satisfy the guiding center approximation. In the following
148 study, we calculate the acceleration rates only at times when κ is greater than 3.
149
150 **3. Results**
151 Figure 1 shows the overview of the MMS observations in a turbulent magnetosheath
152 from 07:08:14 to 07:18:34 UT on 2016 December 18. The location of the MMS
153 spacecraft in the geocentric solar ecliptic (GSE) coordinate system is [11.4, 0.8, 0.2] R_E
154 (R_E is earth radii), downstream of the quasi-perpendicular bow shock. The average
155 spacing of the MMS tetrahedron is ~ 8.5 km ~ 9.5 d_e given the average plasma density
156 of ~ 35 cm^3, where d_e is the electron inertial length. The tetrahedron quality factor (TQF)
157 is ~ 0.99, indicating that the four satellites constitute a nearly perfect tetrahedron in
158 space. One can see from Figures 1a-1c that the electromagnetic fields and plasma flows
159 are highly turbulent. The electron flow speed is similar to that of the ion flow, except
160 that electron bulk velocity has some high-frequency fluctuations, which leads to
161 filamentary currents with peak density larger than 500 nA m^{-2} (Figure 1f). The electron
162 temperature exhibits an anisotropy with $T_{e||}>T_{e\perp}$ in this interval (Figure 1g). The average
163 ion bulk velocity is about 120 km s^{-1} and the average electron temperature is about 50
164 eV.
165 Figure 1g shows that κ is larger than 3 (the black dotted line) for most of the time.
166 This can be also clearly seen in the probability distribution function (PDF) of the κ
167 values displayed in Figure 2a. About 99% of κ are greater than 3, which means that
168 electrons are magnetized almost during the entire interval. The PDF of κ increases from
169 nearly 0 and reaches the peak at around κ=18, then it monotonically descends as the
170 increment of κ. Figures 1h-1j display the electron acceleration rates for the three
171 different acceleration mechanisms. They have both positive and negative values,
172 suggesting bi-directional energy exchange between the electromagnetic fields and
173 electrons rather than unidirectional energy conversion. The largest acceleration rate is
174 up to 2×10^4 eV s^{-1} cm^{-3} ~ 3.2 nW m^{-3}. There are many spikes in accelerated rates, which
175 is the manifestation of intermittency. Note that the above three acceleration rates are

calculated in the frame co-moving with the magnetosheath flow, that is, $\mathbf{E}' = \mathbf{E} + \langle \mathbf{V} \rangle \times \mathbf{B}$, where $\langle \mathbf{V} \rangle$ is the average ion bulk velocity in the whole interval.

To determine the main acceleration mechanism, we plot the PDF of the three acceleration rates in Figure 2b. The total number of data points is about 20,000. We see that the highest value of the PDF is around W=0. The PDFs are sign-indefinite, which implies that the energy exchange between electromagnetic fields and plasmas goes both ways. The PDF of $W_{E||}$ is the broadest among the three, indicating that $E_{||}$ acceleration is generally greater than the other two mechanisms. The PDF of $W_{E||}$ is asymmetric with respect to W=0, with a higher positive tail, while the PDF of W_b shows a subtle heavier negative tail and the PDF of W_f is nearly symmetric to W=0. The average acceleration rate of $E_{||}$, betatron, and Fermi acceleration is 278 eV s^{-1} cm^{-3}, -77 eV s^{-1} cm^{-3}, and -4 eV s^{-1} cm^{-3}, respectively. Therefore, on average, electrons were accelerated by $E_{||}$, whereas betatron and Fermi mechanisms decelerated the electrons. The average energization rate of electrons by $E_{||}$ is at least one order of magnitude larger than the results reported in previous literature (Afshari et al., 2021; Bandyopadhyay et al., 2020). The PDF of $W_{E||}$ is non-Gaussian with a heavier tail (Figure 2c), suggesting the intermittent nature of the acceleration process (Matthaeus et al., 2015). The intermittency is further proved by the large kurtosis of the $E_{||}$, betatron, and Fermi acceleration rate, which is 374, 196, and 72, respectively.

Since the acceleration of electrons is dominated by parallel electric fields, we mainly focus on $E_{||}$ acceleration in the following. To understand at which scale the acceleration occurs, we estimate the spatial scale of the magnetic field $L_{dB} = {}^{B}/_{|\boldsymbol{\nabla B}|}$ using the multi-spacecraft measurements under the assumption that the spatial variation is linear inside the MMS tetrahedron (Chanteur 1998). Here, $|\boldsymbol{\nabla B}|$ is the norm of the Jacobian matrix of the magnetic field, i.e., $|\boldsymbol{\nabla B}| = \sqrt{\sum_{ij}(\frac{\partial B_i}{\partial x_j})^2}$ (Kress et al. 2007). Figure 3a shows the joint PDF of the $E_{||}$ acceleration rate $W_{E||}$ and the L_{dB}. We see that most of the data points are near $W_{E||}$=0, which is consistent with Figure 2b. L_{dB} is typically larger than ~ 0.3 d_i and smaller than 30 d_i. Figure 3b points out that the average acceleration rate descends with the increment of the spatial scale, from larger than 1000 eV s^{-1} cm^{-3}

when $L_{dB} < 10^{-0.5}$ d_i to less than 200 eV s^{-1} cm^{-3} when $L_{dB} > 10$ d_i. Figures 3c displays that the average L_{dB} is the largest near $W_{E||}$=0 and descends toward larger $W_{E||}$ in both the positive and negative directions. The average L_{dB} reduces to about 1 d_i when $W_{E||}$ is 6 times larger than its RMS.

The Partial Variance of Increments (PVI) method has been widely used to identify the coherent structures in turbulent plasma (Matthaeus et al., 2015; Greco et al., 2009, 2018; Chasapis et al., 2015). The PVI index can be calculated using magnetic fields observed by multi-spacecraft:

$$PVI_{ij}(t) = \sqrt{\frac{|B^i(t)-B^j(t)|^2}{\langle |B^i(t)-B^j(t)|^2 \rangle}} \quad (7)$$

where the subscript i, j=1,2,3,4 indicates the different spacecraft. Figure 4a shows the $E_{||}$ acceleration rate conditioned on the PVI index. We see that the average $W_{E||}$ monotonically increases with the increment of PVI index, which means that the most intense $E_{||}$ acceleration corresponds to the largest PVI index. The average $W_{E||}$ with PVI index >3 is about 40 times the $W_{E||}$ averaged over all the data points. We also examine the local increase of the electron temperature conditioned on the PVI index (Figure 4b). The local increase of the electron temperature is represented by the electron temperature normalized by its regional average. It shows that similar to the profile of $W_{E||}$, the average T_e also increases nearly monotonically with the increase of the PVI index. Notice that the monotonic trend is clearer in $Te_{||}$ than in $Te_{\perp}$. This is consistent with previous observations that strong electron heating, measured by the local increase of the electron temperature, occurs within current sheets with large PVI index, while no apparent heating within current sheets with small PVI index (Chasapis et al., 2015; Huang et al., 2022). Here we go one step further by confirming that structures with larger PVI index contribute to greater energy dissipation and electron acceleration.

Moreover, we investigate where the most intense $E_{||}$ acceleration occurs. We define the intense $E_{||}$ acceleration event as the interval in which the peak $W_{E||}$ is greater than 5,100 eV s^{-1} cm^{-3}. This value is the intersection of the PDF of $W_{E||}$ and the Gaussian curve in Figure 2c. The boundary of each event is set as 5100/e ≈ 1,900, where e is the

natural exponential. We identify the coherent structures when the PVI index is larger than the threshold $\langle PVI \rangle + \sigma(PVI) \sim 1.3$, where <PVI> and $\sigma(PVI)$ are the average and standard deviation of PVI index in the entire interval (Greco et al., 2009). Finally, 68 intense $E_{||}$ acceleration events were selected, with 60 events having a PVI index greater than the threshold, i.e., they are within the coherent structures. One can see from Figure 3a that data points with $W_{E||}$ larger than 5,100 eV s^{-1} cm^{-3} are mostly in the range $L_{dB} \sim$ [1, 10] d_i.

Figure 5 shows one example of intense $E_{||}$ acceleration events. It is shown that the intense $E_{||}$ acceleration was coincident with a large PVI index, which corresponds to a coherent structure with a sharp change of the magnetic field and an intense current. A unipolar $E_{||} \sim 3$ mV m^{-1} was responsible for $\sim 8 \times 10^4$ eV s^{-1} cm^{-3} acceleration rate in the parallel direction. Moreover, we transfer the magnetic field, electron bulk flow, and electric current to the local **LMN** coordinates (Figure 5g-5i) to see whether this event was associated with a local reconnection. We employ the same procedure as Man et al. (2022) to identify local reconnection, such as the electron outflowing jets and the out-of-plane current supporting the magnetic field reversal. We see a clear electron bulk flow reversal corresponding well to the current sheet crossing, implying that MMS encountered an active reconnection in this coherent structure. We have further examined all the intense $E_{||}$ acceleration events. Overall, 30 (~ 44%) intense $E_{||}$ acceleration events are associated with local reconnection. Therefore, we conclude that reconnection plays a significant role in accelerating electrons in this event.

4. Discussion and Conclusion

We have analyzed 31 other intervals in the turbulent magnetosheath observed by MMS from the year 2015 to 2019 (Wang et al., 2021). Twenty-two of these intervals are downstream of the quasi-parallel bow shock, and the other 9 events are downstream of the quasi-perpendicular bow shock. These events have a broader range of plasma β. We analyze these events by the same method described in this paper and find qualitatively similar results, that is, electrons are predominantly accelerated by $E_{||}$ no

matter whether the interval is downstream of the quasi-parallel or quasi-perpendicular bow shock.

A further question that needs to be addressed is whether the $E_{||}$ acceleration in the coherent structures is due to Landau damping, stochastic heating, or Joule-type dissipation. Since the electrons are magnetized most of the time, they could not be energized through stochastic heating, which requires that the electron magnetic moment is not conserved (e.g., Vech et al., 2017). This event is different from the events reported by Afshari et al. (2021) and Chen et al. (2019), which demonstrate that electrons were accelerated through Landau resonance with the kinetic Alfven waves. One major difference is that the magnetic field is relatively stable and has few coherent structures in the events studied by Afshari et al. (2021). This is also manifested by the non-Gaussian PDF of the $E_{||}$ acceleration rate in our event, whereas the PDF is near Gaussian in turbulence dominated by Landau damping (not shown). Importantly, we find that the large $E_{||}$ acceleration studied in this paper is usually associated with unipolar $E_{||}$ rather than wave-like $E_{||}$. Thus, the $E_{||}$ acceleration observed in our event is unlikely caused by Landau damping. More detailed analysis using the field-particle correlation technique for each intense $E_{||}$ acceleration event can be performed to further understand $E_{||}$ acceleration in these coherent structures.

In summary, we have investigated how electrons are being accelerated through the dissipation of magnetic energy in nonlinear turbulence in the Earth's magnetosheath. Since electrons are mostly magnetized, we classify the acceleration mechanisms into three types: Fermi process, betatron mechanism, and $E_{||}$ acceleration. We find that the PDF of $E_{||}$ acceleration is significantly broader than the PDF of the other two acceleration rates, which implies that electrons are predominantly accelerated by parallel electric fields. $W_{E||}$ increases with the reduction of the spatial scale and the increment of the PVI index, suggesting that the $E_{||}$ acceleration is the most effective around the ion inertial length and coherent structures play a vital role in energizing electrons through $E_{||}$. We demonstrate that electrons are accelerated through Joule-type dissipation/heating in strong turbulence containing many coherent structures, which is another important building block of the particle energization physical scenario besides

the mechanism proposed by Chen et al. (2019) and Afshari et al. (2021).

The acceleration and heating of ions by turbulence may be quite different to the electrons because ions are expected to be demagnetized due to their much larger gyro-radius. Hence one cannot use the guiding center approximation to describe the ion motion and may resort to other methods to quantify the ion acceleration, which is underway for further report.

Acknowledgments

Thanks to the MMS team for providing the high-quality data to complete this work. This work is supported by the National Natural Science Foundation of China (NSFC) under grant Nos. 42074197, 42130211, and 41774154.

Data Availability Statement

The data used in this study was obtained from the MMS Science Data Center (https://lasp.colorado.edu/mms/sdc/public/about/browse-wrapper/).

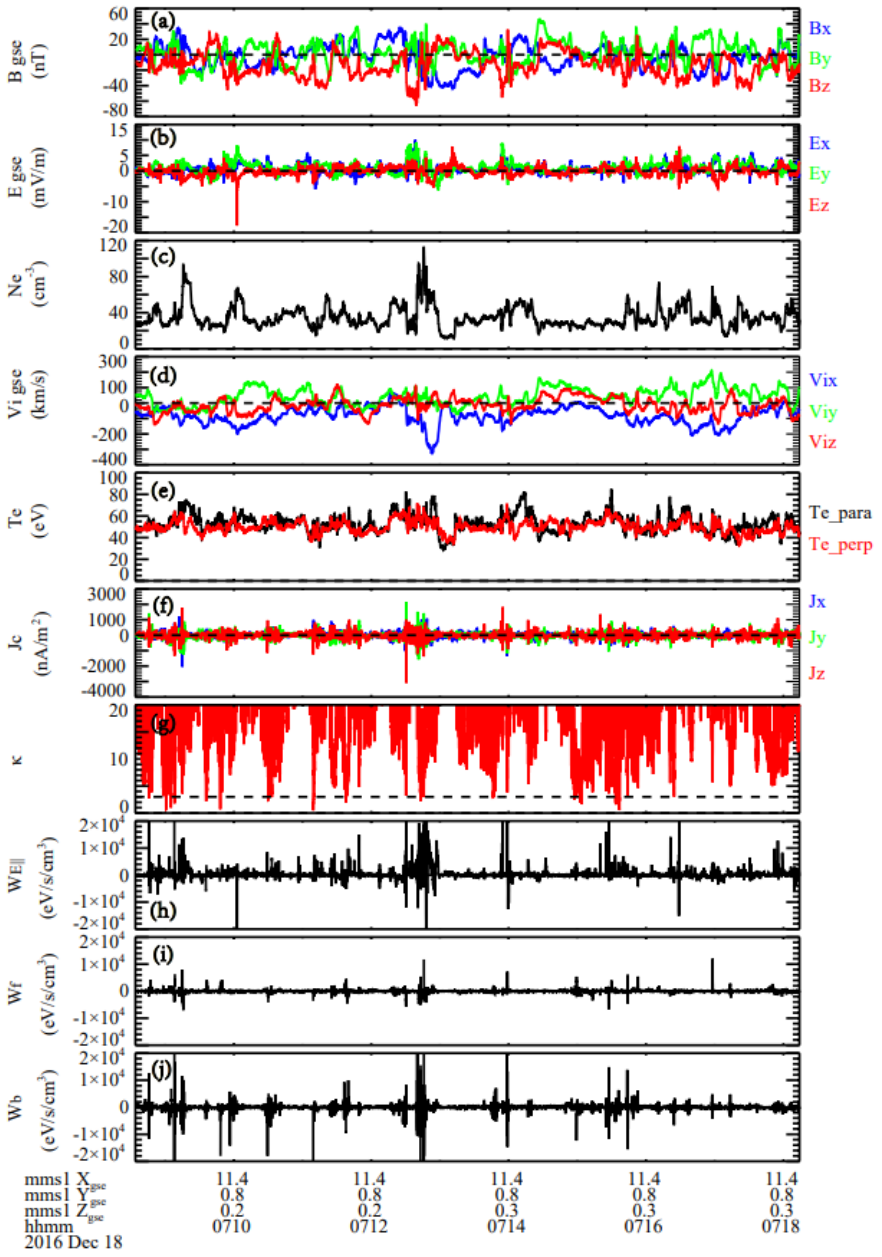

Figure 1. Overview of the turbulence in the magnetosheath observed by MMS from 07:08:14 to 07:18:34 UT on 18 December 2016. From the top to bottom are: (a) three components of the magnetic field and (b) the electric field; (c) electron number density; (d) ion bulk velocity; (e) electron parallel and perpendicular temperatures; (f) electric current density; (g) κ value; (h) – (j) the acceleration rate from $E_{||}$, Fermi process and betatron mechanism, respectively. The vectors are displayed in the GSE coordinate system.

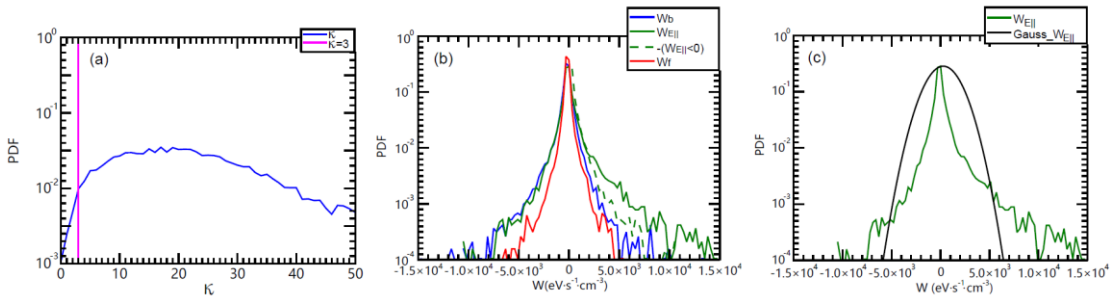

316

317 **Figure 2.** (a) probability distribution function (PDF) of κ. The pink line marks κ=3; (b)
318 PDF of betatron acceleration rate (blue), Fermi acceleration rate (red) and the $E_{||}$
319 acceleration rate (green). The green dashed line is the mirror image of the negative $E_{||}$
320 acceleration rate; (c) comparison of the PDF of the $E_{||}$ acceleration rate and the Gaussian
321 curve (black).

322

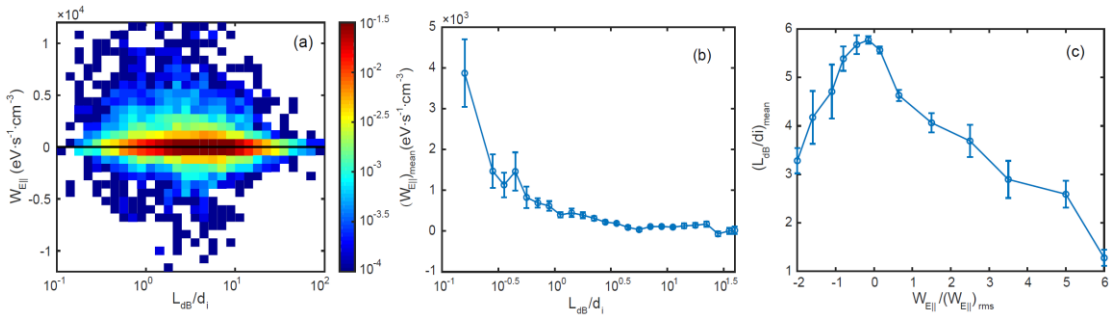

323

324 **Figure 3.** (a) Joint PDFs of $E_{||}$ acceleration rate and the local magnetic field scale L_{dB};
325 (b) the average $W_{E||}$ as a function of L_{dB}; (c) the average L_{dB} as a function of
326 $W_{E||}/(W_{E||})_{rms}$, here $(W_{E||})_{rms}$ is the root mean square of $W_{E||}$; The vertical bars in panels
327 (b) and (c) represent the standard errors of the mean.

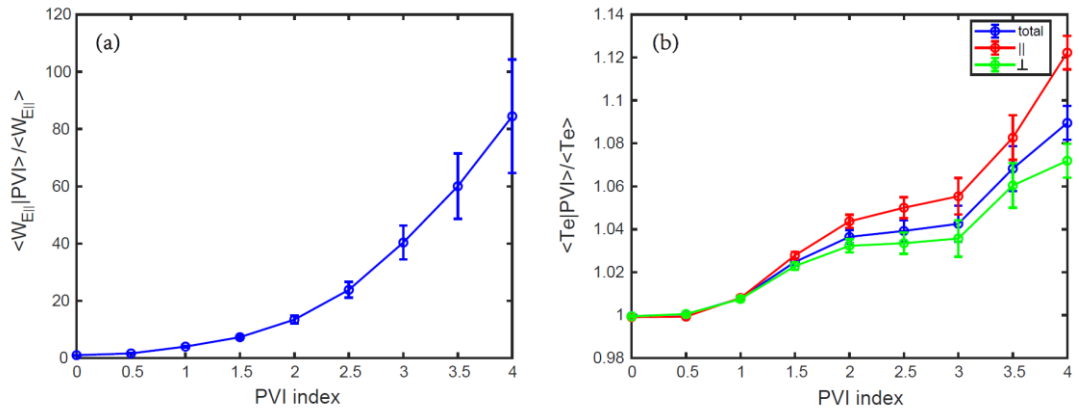

328

329 **Figure 4.** Average $E_{||}$ acceleration rate (a) and electron temperature (b) conditioned on
330 the binned PVI index. The average $W_{E||}$ is normalized by the averaged value in the entire

interval. The electron temperature is normalized by $<T_e>$ in a moving window with duration of 4 s, equivalent to approximately 10 d_i. The vertical bars represent the standard error of the mean.

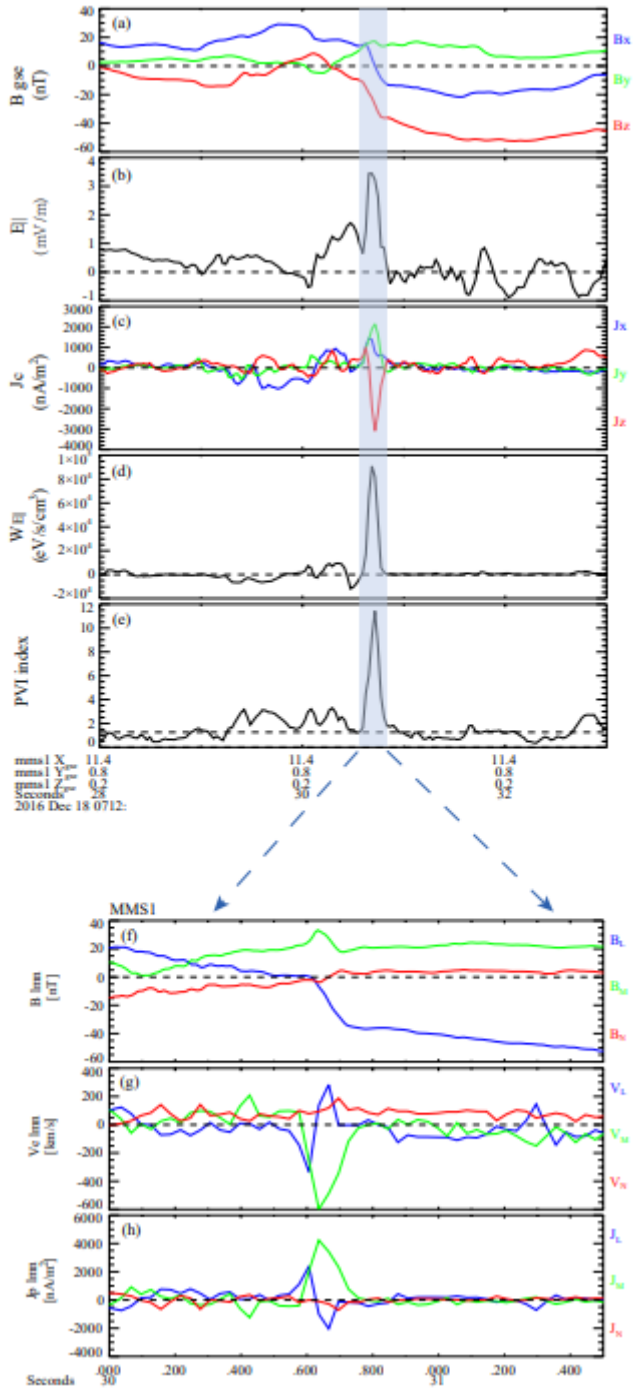

Figure 5. An example of the intense $E_{||}$ accelerate event. From the top to bottom are: (a) three components of the magnetic field; (b) parallel electric field; (c) electric current density; (d) $E_{||}$ acceleration rate; (e) PVI Index. The shaded area highlights a significant

electron accelerate by $E_{||}$ within a coherent structure. The expanded view displays the (f) magnetic field; (g) electron bulk velocity and (h) current density in the **LMN** coordinate system around the coherent structure.

References

[1] Afshari, A. S., Howes, G. G., Kletzing, C. A., Hartley, D. P., & Boardsen, S. A. (2021). The importance of electron Landau damping for the dissipation of turbulent energy in terrestrial magnetosheath plasma. Journal of Geophysical Research: Space Physics, 126(12), e2021JA029578. https://doi.org/10.1029/2021JA02957

[2] Alexandrova, O., & Saur, J. (2008). Alfvén vortices in Saturn's magnetosheath: Cassini observations. Geophysical Research Letters, 35(15). https://doi.org/10.1029/2008GL034411

[3] Bandyopadhyay, R., Matthaeus, W. H., Parashar, T. N., Yang, Y., Chasapis, A., Giles, B. L., Gershman, D. J., Pollock, C. J., Russell, C. T., Strangeway, R. J., Torbert, R. B., Moore, T. E., & Burch, J. L. (2020). Statistics of kinetic dissipation in Earth's magnetosheath: MMS observations. Physical Review Letters, 124(25), 255101. https://doi.org/10.1103/PhysRevLett.124.255101

[4] Bowen, T. A., Chandran, B. D., Squire, J., Bale, S. D., Duan, D., Klein, K. G., Larson, D., Mallet, A., McManus, M. D., Meyrand, R., et al. (2022). In Situ Signature of Cyclotron Resonant Heating in the Solar Wind. Physical Review Letters, 129(16), 165101.

[5] Büchner, J., & Zelenyi, L. M. (1989). Regular and chaotic charged particle motion in magnetotaillike field reversals: 1. Basic theory of trapped motion. Journal of Geophysical Research Space Physics, 94(A9), 11821-11842. https://doi.org/10.1029/JA094iA09p11821

[6] Chandran, B., Li, B., Rogers, B., Quataert, E., & Germaschewski, K. (2010). Perpendicular ion heating by low-frequency Alfven-wave turbulence in the solar wind. The Astrophysical Journal, 720(1). https://doi.org/10.1088/0004-637X/720/1/503

[7] Chanteur, G. (1998). Spatial interpolation for four spacecraft: Theory. In G.

368 Paschmann, P. W. Daly (Eds.), Analysis methods for multi-spacecraft data (p. 349).
369 Noordwijk, Netherlands: ESA Publ. Div.
370 [8] Chasapis, A., Retinò, A., Sahraoui, F., Vaivads, A., Khotyaintsev, Y. V., Sundkvist,
371 D., Greco, A., Valvo, L. S., & Canu, P. (2015). Thin current sheets and associated
372 electron heating in turbulent space plasma. The Astrophysical Journal Letters, 804(1),
373 L1. https://doi.org/10.1088/2041-8205/804/1/L1
374 [9] Chen, C. H. K. (2016). Recent progress in astrophysical plasma turbulence from
375 solar wind observations. Journal of Plasma Physics, 82(6).
376 https://doi.org/10.1017/S0022377816001124
377 [10] Chen, C. H. K., Klein, K. G., & Howes, G. G. (2019). Evidence for electron Landau
378 damping in space plasma turbulence. Nature communications, 10(1), 1-8.
379 https://doi.org/10.1038/s41467-019-08435-3
380 [11] Dahlin, J. T., Drake, J. F., & Swisdak, M. (2014). The mechanisms of electron
381 heating and acceleration during magnetic reconnection. Physics of Plasmas, 21(9),
382 092304. https://doi.org/10.1063/1.4894484
383 [12] Dmitruk, P., Matthaeus, W. H., & Lanzerotti, L. J. (2004a). Discrete modes and
384 turbulence in a wave-driven strongly magnetized plasma. Geophysical Research Letters,
385 31(21). https://doi.org/10.1029/2004GL021119
386 [13] Dmitruk, P., Matthaeus, W. H., & Seenu, N. (2004b). Test particle energization by
387 current sheets and nonuniform fields in magnetohydrodynamic turbulence. The
388 Astrophysical Journal, 617(1), 667. https://doi.org/10.1086/425301
389 [14] Ergun, R. E., Tucker, S., Westfall, J., Goodrich, K. A., Malaspina, D. M., Summers,
390 D., Wallace, J., Karlsson, M., Mack, J., Brennan, N., Pyke, B., Withnell, P., Torbert, R.,
391 Macri, J., Rau, D., Dors, I., Needell, J., Lindqvist, P. -A., Olsson, G., Cully, C. M. (2016).
392 The axial double probe and fields signal processing for the MMS mission. Space
393 Science Reviews, 199(1), 167–188. https://doi.org/10.1007/s11214-014-0115-x
394 [15] Gary, S. P., Winske, D., & Hesse, M. (2000). Electron temperature anisotropy
395 instabilities: Computer simulations. Journal of Geophysical Research: Space Physics,
396 105(A5), 10751-10759. https://doi.org/10.1029/1999JA000322
397 [16] Greco, A., Matthaeus, W. H., Perri, S., Osman, K. T., Servidio, S., Wan, M., &

Dmitruk, P. (2018). Partial variance of increments method in solar wind observations and plasma simulations. Space Science Reviews, 214(1), 1-27. https://doi.org/10.1007/s11214-017-0435-8

[17] Greco, A., Matthaeus, W. H., Servidio, S., Chuychai, P., & Dmitruk, P. (2009). Statistical analysis of discontinuities in solar wind ACE data and comparison with intermittent MHD turbulence. The Astrophysical Journal, 691(2), L111. https://doi.org/10.1088/0004-637X/691/2/L111

[18] He, J., Pei, Z., Wang, L., Tu, C., Marsch, E., Zhang, L., & Salem, C. (2015). Sunward propagating Alfvén waves in association with sunward drifting proton beams in the solar wind. The Astrophysical Journal, 805(2), 176. https://doi.org/10.1088/0004-637X/805/2/176

[19] He, J., Wang, L., Tu, C., Marsch, E., & Zong, Q. (2015). Evidence of Landau and cyclotron resonance between protons and kinetic waves in solar wind turbulence. The Astrophysical Journal Letters, 800(2), L31. https://doi.org/10.1088/2041-8205/800/2/L31

[20] Howes, G. G. (2017). A prospectus on kinetic heliophysics. Physics of Plasmas, 24(5), 055907. https://doi.org/10.1063/1.4983993

[21] Huang, S. Y., Sahraoui, F., Retinò, A., Le Contel, O., Yuan, Z. G., Chasapis, A., Aunai, N., Breuillard, H., Deng, X. H., Zhou, M., et al. (2016). MMS observations of ion-scale magnetic island in the magnetosheath turbulent plasma. Geophysical Research Letters, 43(15), 7850-7858. https://doi.org/10.1002/2016GL07003

[22] Huang, S. Y., Du, J. W., Sahraoui, F., Yuan, Z. G., He, J. S., Zhao, J. S., Le Contel, O., Breuillard, H., Wang, D. D., Yu, X. D., et al. (2017a). A statistical study of kinetic-size magnetic holes in turbulent magnetosheath: MMS observations. Journal of Geophysical Research: Space Physics, 122(8), 8577-8588. https://doi.org/10.1002/2017JA024415

[23] Huang, S. Y., Sahraoui, F., Yuan, Z. G., He, J. S., Zhao, J. S., Le Contel, O., Deng, X. H., Zhou, M., Fu, H. S., Shi, Q.Q., et al. (2017b). Magnetospheric multiscale observations of electron vortex magnetic hole in the turbulent magnetosheath plasma. The Astrophysical Journal Letters, 836(2), L27. https://doi.org/10.3847/2041-

8213/aa5f50

[24] Huang, S. Y., Zhang, J., Sahraoui, F., Yuan, Z. G., Deng, X. H., Jiang, K., Xu, S. B., Wei, Y. Y., He, L. H., & Zhang, Z. H. (2020). Observations of magnetic field line curvature and its role in the space plasma turbulence. The Astrophysical Journal Letters, 898(1), L18. https://doi.org/10.3847/2041-8213/aba263

[25] Huang, S. Y., Zhang, J., Yuan, Z. G., Jiang, K., Wei, Y. Y., Xu, S. B., et al. (2022). Intermittent dissipation at kinetic scales in the turbulent reconnection outflow. Geophysical Research Letters, 49, e2021GL096403. https://doi.org/10.1029/2021GL096403

[26] Isenberg, P. A. (2001). The kinetic shell model of coronal heating and acceleration by ion cyclotron waves: 2. Inward and outward propagating waves. Journal of Geophysical Research: Space Physics, 106(A12), 29249-29260. https://doi.org/10.1029/2001JA000176

[27] Isenberg, P. A., & Hollweg, J. V. (1983). On the preferential acceleration and heating of solar wind heavy ions. Journal of Geophysical Research: Space Physics, 88(A5), 3923-3935. https://doi.org/10.1029/JA088iA05p03923

[28] Kiyani, K. H., Osman, K. T., & Chapman, S. C. (2015). Dissipation and heating in solar wind turbulence: From the macro to the micro and back again. Philosophical Transactions of the Royal Society A: Mathematical, Physical and Engineering Sciences, 373(2041), 20140155. https://doi.org/10.1098/rsta.2014.0155

[29] Klein, K. G., Howes, G. G., & TenBarge, J. M. (2017). Diagnosing collisionless energy transfer using field–particle correlations: gyrokinetic turbulence. Journal of Plasma Physics, 83(4). https://doi.org/10.1017/S0022377817000563

[30] Kress, B. T., Hudson, M. K., Looper, M. D., Albert, J., Lyon, J. G., & Goodrich, C. C. (2007). Global MHD test particle simulations of> 10 MeV radiation belt electrons during storm sudden commencement. Journal of Geophysical Research: Space Physics, 112(A9). https://doi.org/10.1029/2006JA012218

[31] Lindqvist, P. A., Olsson, G., Torbert, R. B., King, B., Granoff, M., Rau, D., Needell, G., Turco, S., Dors, I., Beckman, P., et al. (2016). The spin-plane double probe electric field instrument for MMS. Space Science Reviews, 199(1), 137-165.

https://doi.org/10.1007/s11214-014-0116-9

[32] Ma, W., Zhou, M., Zhong, Z., & Deng, X. (2020). Electron acceleration rate at dipolarization fronts. The Astrophysical Journal, 903(2), 84. https://doi.org/10.3847/1538-4357/abb8cc

[33] Ma, W., Zhou, M., Zhong, Z., & Deng, X. (2022). Contrasting the Mechanisms of Reconnection-driven Electron Acceleration with In Situ Observations from MMS in the Terrestrial Magnetotail. The Astrophysical Journal, 931(2), 135. https://doi.org/10.3847/1538-4357/ac6be6

[34] Man, H., Zhou, M., Zhong, Z., & Deng, X. (2022). Intense energy conversion events at the magnetopause boundary layer. Geophysical Research Letters, 49(8), e2022GL098069. https://doi.org/10.1029/2022GL098069

[35] Marsch, E., & Tu, C. Y. (2001). Evidence for pitch angle diffusion of solar wind protons in resonance with cyclotron waves. Journal of Geophysical Research: Space Physics, 106(A5), 8357-8361. https://doi.org/10.1029/2000JA000414

[36] Matthaeus, W. H., Wan, M., Servidio, S., Greco, A., Osman, K. T., Oughton, S., & Dmitruk, P. (2015). Intermittency, nonlinear dynamics and dissipation in the solar wind and astrophysical plasmas. Philosophical Transactions of the Royal Society A: Mathematical, Physical and Engineering Sciences, 373(2041), 20140154. https://doi.org/10.1098/rsta.2014.0154

[37] Osman, K. T., Matthaeus, W. H., Gosling, J. T., Greco, A., Servidio, S., Hnat, B., Chapman, S. C., & Phan, T. D. (2014). Magnetic reconnection and intermittent turbulence in the solar wind. Physical Review Letters, 112(21), 215002. https://doi.org/10.1103/PhysRevLett.112.215002

[38] Osman, K. T., Matthaeus, W. H., Wan, M., & Rappazzo, A. F. (2012). Intermittency and local heating in the solar wind. Physical review letters, 108(26), 261102. https://doi.org/10.1103/PhysRevLett.108.261102

[39] Pollock, C., Moore, T., Jacques, A., Burch, J., Gliese, U., Saito, Y., Omoto, T., Avanov, L., Barrie, A., Coffey, V., et al. (2016). Fast plasma investigation for magnetospheric multiscale. Space Science Reviews, 199(1), 331-406. https://doi.org/10.1007/s11214-016-0245-4

[40] Retinò, A., Sundkvist, D., Vaivads, A., Mozer, F., André, M., & Owen, C. J. (2007). In situ evidence of magnetic reconnection in turbulent plasma. Nature Physics, 3(4), 235-238. https://doi.org/10.1038/nphys574

[41] Russell, C. T., Anderson, B. J., Baumjohann, W., Bromund, K. R., Dearborn, D., Fischer, D., Le, G., Leinweber, H. K., Leneman, D., Magnes, W., et al. (2016). The magnetospheric multiscale magnetometers. Space Science Reviews, 199(1), 189-256. https://doi.org/10.1007/s11214-014-0057-3

[42] Sahraoui, F., Goldstein, M. L., Robert, P., & Khotyaintsev, Y. V. (2009). Evidence of a cascade and dissipation of solar-wind turbulence at the electron gyroscale. Physical Review Letters, 102(23), 231102. https://doi.org/10.1103/PhysRevLett.102.231102

[43] Vech, D., Klein, K. G., & Kasper, J. C. (2017). Nature of stochastic ion heating in the solar wind: testing the dependence on plasma beta and turbulence amplitude. The Astrophysical Journal Letters, 850(1), L11. https://doi.org/10.3847/2041-8213/aa9887

[44] Wang, Y., Bandyopadhyay, R., Chhiber, R., Matthaeus, W. H., Chasapis, A., Yang, Y., Wilder, F. D., Gershman, D. J., Giles, B. L., Pollock, C. J., et al. (2021). Statistical survey of collisionless dissipation in the terrestrial magnetosheath. Journal of Geophysical Research: Space Physics, 126(6), e2020JA029000. https://doi.org/10.1029/2020JA029000

[45] Yao, S. T., Shi, Q. Q., Guo, R. L., Yao, Z. H., Tian, A. M., Degeling, A. W., Sun, W. J., Liu, J., Wang, X. G., Zong, Q. G., et al. (2018). Magnetospheric Multiscale observations of electron scale magnetic peak. Geophysical Research Letters, 45(2), 527-537. https://doi.org/10.1002/2017GL075711

[46] Zhong, Z. H., Zhou, M., Huang, S. Y., Tang, R. X., Deng, X. H., Pang, Y., & Chen, H. T. (2019). Observations of a kinetic-scale magnetic hole in a reconnection diffusion region. Geophysical Research Letters, 46(12), 6248-6257. https://doi.org/10.1029/2019GL082637

[47] Zhong, Z. H., Zhou, M., Tang, R. X., Deng, X. H., Turner, D. L., Cohen, I. J., Pang, Y., Man, H. Y., Russell, C. T., Giles, B. L., et al. (2020). Direct evidence for electron acceleration within ion-scale flux rope. Geophysical Research Letters, 47(1), e2019GL085141. https://doi.org/10.1029/2019GL085141

[48] Zhou, M., El-Alaoui, M., Lapenta, G., Berchem, J., Richard, R. L., Schriver, D., & Walker, R. J. (2018). Suprathermal electron acceleration in a reconnecting magnetotail: Large-scale kinetic simulation. Journal of Geophysical Research: Space Physics, 123(10), 8087-8108. https://doi.org/10.1029/2018JA025502

[49] Zhou, M., Man, H. Y., Deng, X. H., Pang, Y., Khotyaintsev, Y., Lapenta, G., Yi, Y. Y., Zhong, Z. H., Ma, W. Q. (2021). Observations of secondary magnetic reconnection in the turbulent reconnection outflow. Geophysical Research Letters, 48(4), e2020GL091215. https://doi.org/10.1029/2020GL091215